Purdue University

Purdue e-Pubs

International Refrigeration and Air Conditioning Conference

School of Mechanical Engineering

2021

Permeability Analysis of Additively-Manufactured Wick Structures with Heat Exchanger Applications

Jordan Alexander Morrow
Kansas State University, United States of America, jordan17@ksu.edu

Carlos Espino Mendez

Melanie M Derby

Follow this and additional works at: https://docs.lib.purdue.edu/iracc

Permeability Analysis of Additively-Manufactured Wick Structures with Heat Exchanger Applications

Jordan MORROW[1]*, Carlos ESPINO MENDEZ[1], Melanie DERBY[1]

[1]Kansas State University, Alan Levin Department of Mechanical and Nuclear Engineering,
Manhattan, KS, USA
jordan17@ksu.edu, espino4@ksu.edu, derbym@ksu.edu

* Corresponding Author

ABSTRACT

Heat pipes and other heat transfer applications use capillary-driven liquid motion to enhance performance. This research uses water and a low surface tension fluid FC-40 to test additive-manufactured polymer wicks using a rate-of-rise test. The rate-of-rise tests give a measure of the wicks' performance capabilities as well as being able to calculate the wicks' permeability and effective pore radius. Four wicks were measured having two different internal structures (i.e., 1.0 mm triangle and 1.75 mm square) and two external structures (i.e., layered and column). The 1.0 mm Triangle wicks performed better than their 1.0 mm Square counterparts for both water and FC-40. Both 1.0 mm Triangle wicks performed similarly for both water and FC-40, with the column wick (11.0 mm) performing better than the layered wick (8.98 mm). Using a least squares method from the rate-of-rise results, the permeability and effective pore radius of each wick were calculated for the 1.0 mm triangle layered wick, the 1.75 mm square layered wick, and the 1.0 mm triangle column wick. The 1.75 mm square column wick was unable to wick either liquid, so the permeability and effective pore radius were not able to be calculated. The permeability and effective pore radius for each wick were 3.00 um^2 and 130.1 um, 0.95 um^2 and 221.1 um, and 77.8 um^2 and 1099 um, respectively. Some challenges involved with polymer additive manufacturing design and creation were also discussed.

1. INTRODUCTION

Heat transfer applications such as heat pipes, vaper chambers, and electronics cooling have used capillary-driven liquid motion to enhance heat transfer performance (e.g., preventing dryout in boiling). The wick geometry and properties of the fluid affect maximum capillary transport (Albu *et al.*, 2019; Esarte *et al.*, 2017; Horner *et al.*, 2014; Huang *et al.*, 2017; Jafari *et al.*, 2017, 2018; Li & Peterson, 2006; Li *et al.*, 2006; Ravi *et al.*, 2014; Tang *et al.*, 2010). Studies on parameters that impact wick efficiency – porosity, permeability, and capillarity – have been done on various types of porous media (e.g., micro-pillars and carbon nanotubes, meshes and sintered wicks, and additively-manufactured porous structures). Researchers studied micro-pillar and carbon nanotube wick structures for evaporation applications. In one study, the evaporation dryout threshold was impacted by pillar spacing, but not pillar diameter; the geometry of the micro-pillar wick can be optimized for unique wicking lengths (Horner *et al.*, 2014). Another study observed capillary pressure in micro-pillar wicks was controlled by *x*- and *y*-direction pillar spacing ratios; however, *x*-direction pillar spacing ratios had more impact on permeability than *y*-direction pillar spacing ratios. Maximizing heat pipe velocity was optimum at low *y*-direction pillar spacing ratios and high pillar height ratios. Heat pipes with rectangular micro-pillars have higher cooling capacities and velocities than square micro-pillar arrays (Hale *et al.*, 2014). Evaporation dryout heat flux can be optimized through pillar diameter and spacing; dryout heat flux also scales with pillar thickness (Adera *et al.*, 2016).

Capillary action is a critical mechanism in meshes and sintered wicks. Sintered copper structures for evaporation had increasing heat transfer coefficients as heat flux increased until dryout, where the heat transfer coefficients decreased. The critical heat flux increased as the sintered wick wall thickness increased (up to 1 mm thick), but wall thickness has no impact on the heat transfer coefficient. The copper sintered structures had three times higher critical heat flux than a smooth copper surface, and the critical heat flux was affected by the capillary limit of the sintered structure (Li *et al.*, 2006). Sintered metal powder wicks were used, along with carbon paper wicks, to present a method of calculating the permeability and effective pore radius of a porous structure using rate-of-rise tests (Holley & Faghri,
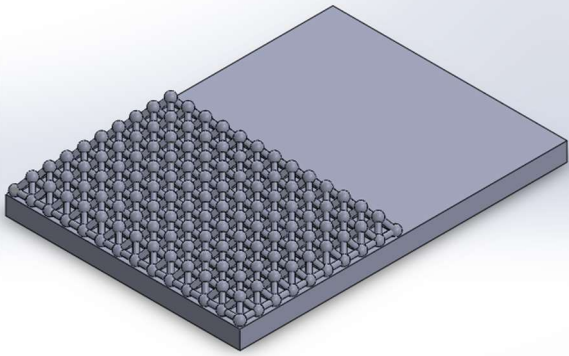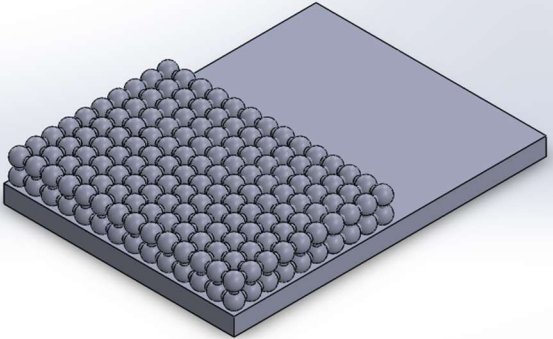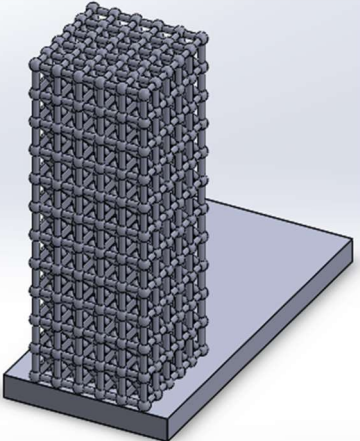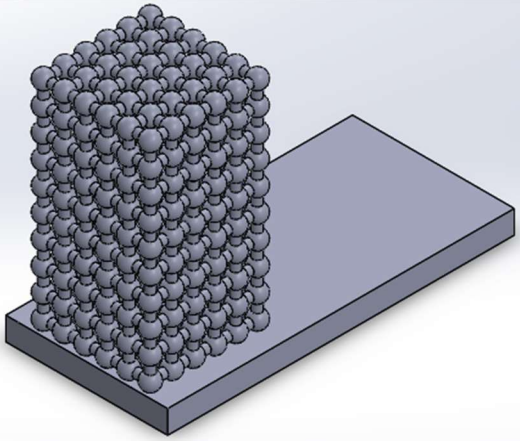
2006). Copper composite wicks (i.e., grooved wicks made of sintered copper particles) studied using an infrared camera were found to have higher capillary force than grooved wicks or sintered particle wicks (Tang *et al.*, 2010). Aluminum grooved wicks subjected to alkaline corrosion treatment showed 155 percent increase over non-corroded aluminum grooved wicks (Huang *et al.*, 2017). Copper sintered wicks composed of two spherical particle sizes (i.e., 100 um and 200 um) were found to have enhanced permeability and wicking ability than uniform particle (i.e., only 100 um or only 200 um) sintered wicks.

In recent years, metal additive manufacturing has been used to create porous structures for heat pipe applications. A stainless-steel rectangular-shaped porous structure was created using selective laser melting technology. One study investigated the effective thermal conductivity and contact angle of the porous structure (Jafari *et al.*, 2017); they later measured the capillary performance (i.e., permeability/effective pore radius) of the additive-manufactured wick, noting the large permeability as reason for the enhanced capillary performance compared to other wick structures (i.e., sintered, mesh, or composite wicks) (Jafari *et al.*, 2018). Another additive-manufactured stainless steel wick was used as the primary wick in a loop heat pipe. The case study done with this wick in a loop heat pipe cooling an 80-watt streetlamp showed a 10 percent increase in heat transfer rate over a loop heat pipe with a conventional primary wick.

The objectives of this research are to understand how controllable factors (i.e., permeability and effective pore radius) impact wick performance and to discuss the tradeoffs involved in wick performance and wick manufacturing.

2. EXPERIMENTAL APPARATUS

Table 1: Schematics of wicks tested: 1.0 mm Triangle Layered (upper left), 1.75 mm Square Layered (upper right), 1.0 mm Triangle Column (lower left), and 1.75 mm Square Column (lower left)

The additive-manufactured polymer wicks used in this study were printed on a Stratasys Polyjet printer with a layer resolution of 280 μm. The wicks were printed out of Rigur450 material. Table 1 shows schematics of all four wicks

tested. The test wicks were designed in two internal structures and two external structures. The two internal structures are 1.5 mm spheres connected in a simple cubic structure (left side of Table 1) and 1.0 mm spheres connected in a body-centered cubic structure (right side of Table 1). The spheres of both wick structures were connected by small connecting rods. The two external structures are a 2-layer wick with the support base oriented vertically along the back of the wick (top row of Table 1) and a column wick with the support base oriented horizontally at the top of the wick (bottom row of Table 1).

2.1 Rate-of-rise tests
Rate-of-rise tests were conducted based on the procedure described in Holley and Faghri (2006) using water and FC-40. Figure 1 shows a schematic of the experimental apparatus. Each structure was clamped to a stand with a petri dish sitting on an adjustable micrometer platform below the wick structure. The fluid was placed in the dish and slowly raised until the fluid slightly touched the bottom layer of the wick structures. Once the fluid and the wicks met, the movement was stopped to allow transport through capillary forces, as recorded by a high-speed camera (Fastech IL3 with Leica Z16 APO lens) for video analysis using FASTCAM viewer (PFV4). Each wick was tested with one fluid, then blown out with compressed air and let to dry overnight to ensure the wick was completely devoid of fluid before the next test.
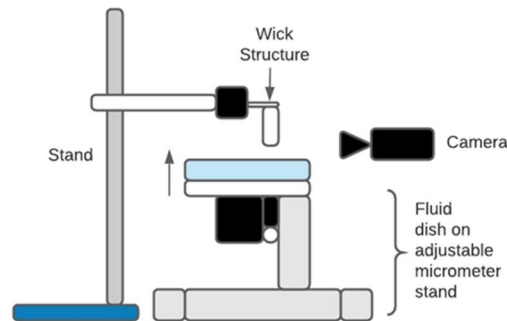

Figure 1: Rate-of-rise experimental apparatus

2.2 Rate-of-rise analyses
The videos from the rate-of-rise tests were analyzed using PFV4 to track the rise of the fluid into the wick. Using the data from the video, the rate of rise was plotted as height risen in millimeters versus time in seconds. These plots can be found in the next section. The max height and time taken for the fluid to reach the max height were used to calculate the permeability and effective pore radius. The porosity of each wick is calculated as

$$\epsilon = \frac{1 - V_{solid}}{V_{total}} \tag{1}$$

where V_{solid} is the volume of the solid structure of the wick and V_{total} is the total volume occupied by the wick. Inside the wick, there is a balance of three forces, represented as pressures, that are acting on the fluid affecting how the fluid moves through the wick.

$$\Delta P_{cap} = \frac{2\sigma}{r_{eff}} \tag{2}$$

$$\Delta P_{hs} = -\rho g x \tag{3}$$

$$\Delta P_f = -\frac{\mu\epsilon}{K} x \frac{dx}{dt} \tag{4}$$

The capillary pressure (2) pulls the fluid up into the wick. Resisting the upward flow of the fluid are the hydrostatic pressure (3) and the pressure loss due to friction (4) of the fluid flowing along the wick surface. In Equations 2 – 4, σ is the surface tension of the fluid, r_{eff} is the effective pore radius of the wick, ρ is the liquid density of the fluid, g is the gravitational constant, x is the height the fluid pulled into the wick, μ is the liquid viscosity of the fluid, ε is the porosity of the wick, K is the permeability of the wick, and t is the time it takes the fluid to pull into the wick. Balancing these three pressures creates a differential equation, which can be solved assuming only height changes with time (Equation 5).

$$-\left[\frac{2\sigma}{r_{eff}} \ln\left(1 - \frac{\rho g r_{eff}}{2\sigma} x\right) + \rho g x \right] = \frac{K\rho^2 g^2}{\epsilon\mu} t \tag{5}$$

Equation 5 has two unknowns (i.e., permeability and effective pore radius) and is solved using a least squares method. The theoretical time taken for the give height is calculated using a range of permeability and effective pore radius values. The mean absolute deviation is calculated and is used to find the permeability-effective pore radius combination that gives the lowest mean absolute deviation.

3. Results and Discussion

3.1 Rate-of-Rise Results
Experiments were conducted on both style of wicks. Figures 2 through 9 show the fluids wicking up each of the four structures. Figures 2 through 7 show successful wicking into the structure. Figure 8 and 9 show the fluid sit at the base of the wick and not move into the pores of the wick.
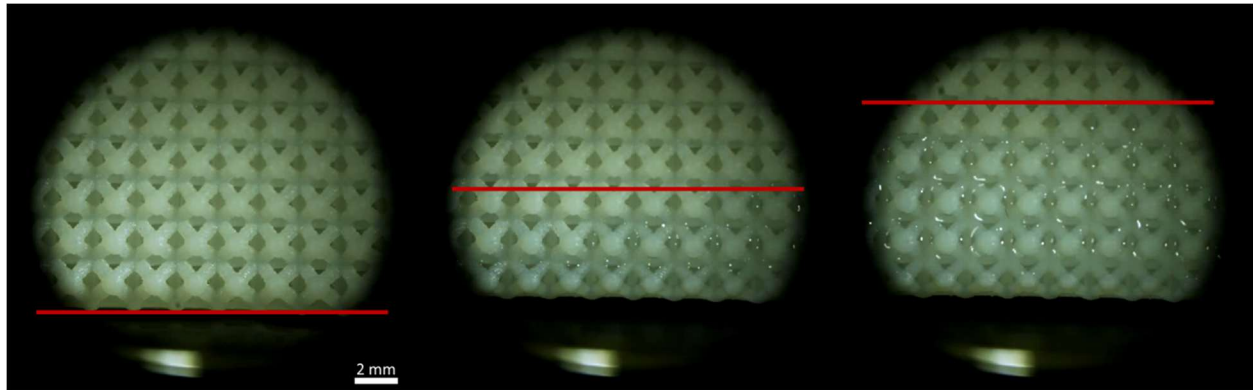

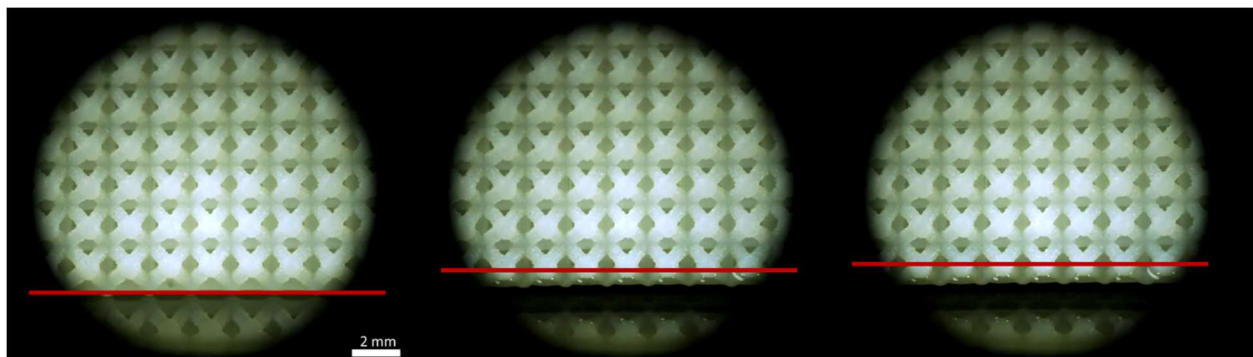**Figure 2:** Water wicking into 1.0 mm triangle layered wick

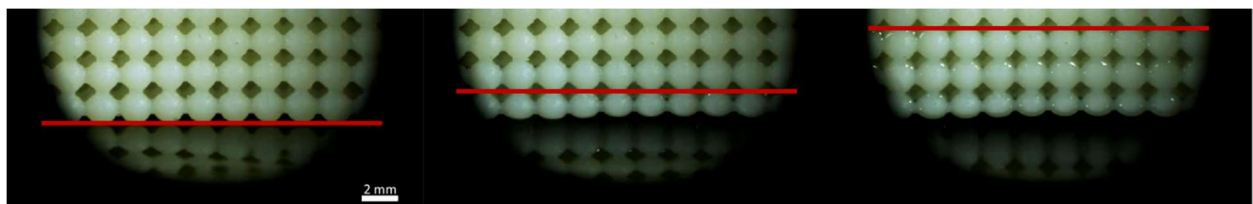**Figure 3:** FC-40 wicking into 1.0 mm triangle layered wick

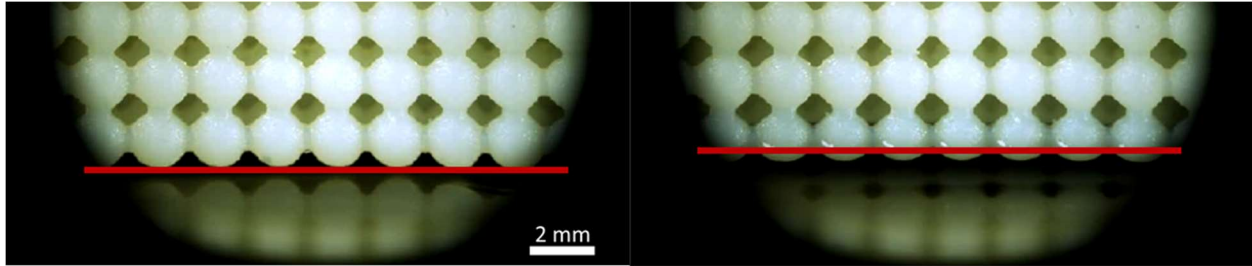**Figure 4:** Water wicking into 1.75 mm square layered wick

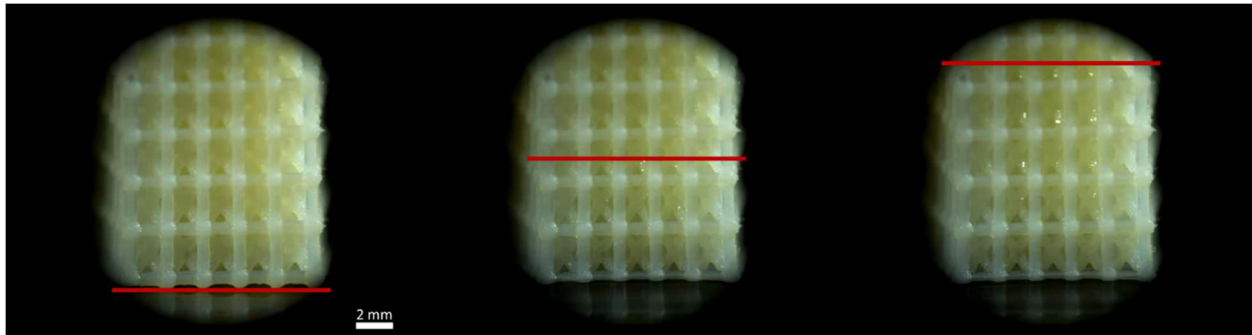**Figure 5:** FC-40 wicking into 1.75 mm square layered wick

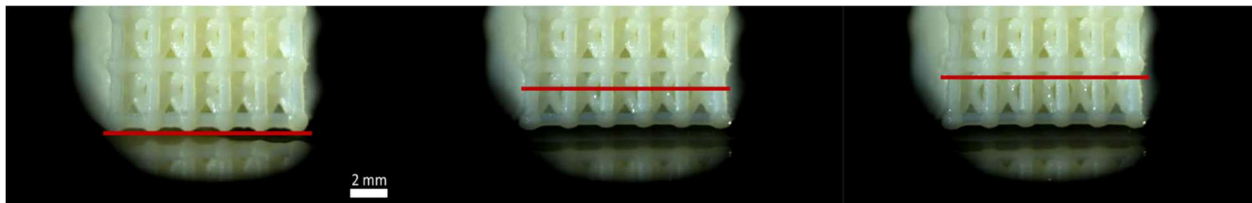**Figure 6:** Water wicking into 1.0 mm triangle column wick

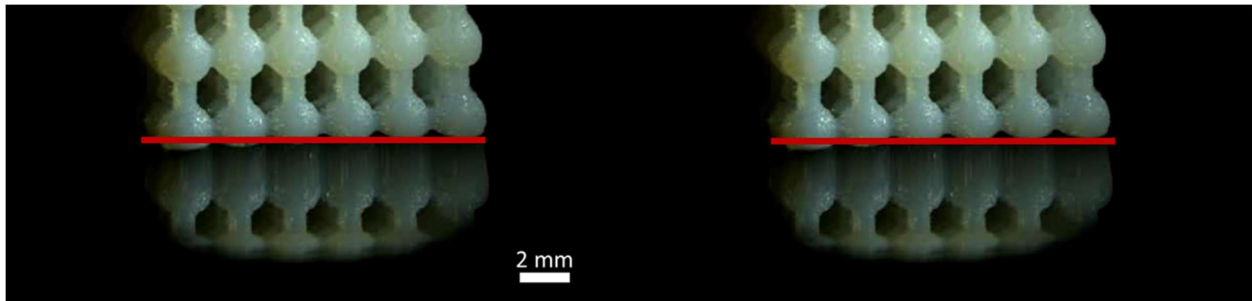**Figure 7:** FC-40 wicking into 1.0 mm triangle column wick

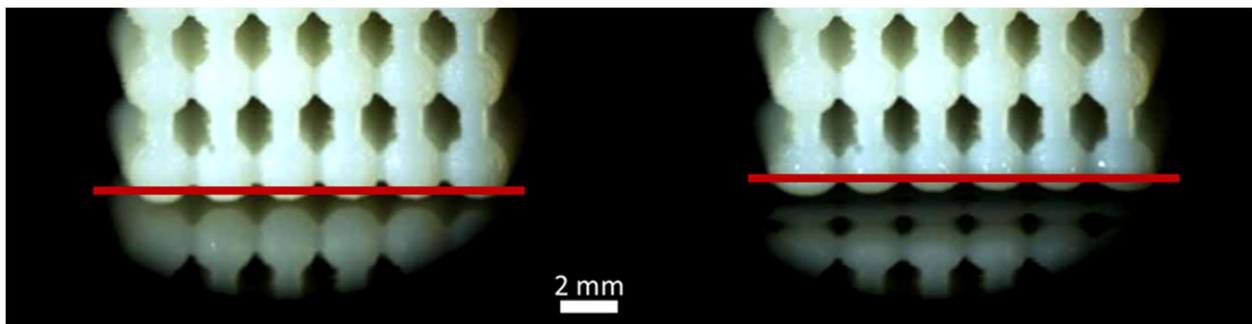**Figure 8:** Water wicking into 1.75 mm square column wick

Figure 9: FC-40 wicking into 1.75 mm square column wick

Figure 10 shows the rate at which the fluid rose in the 1.0 mm triangle wick with respect to time. The layered wick (left) and the column wick (right) show similar trends to each other for both water and FC-40. The max height when using water was 8.98 mm (layered) and 11.0 mm (column). The max height when using FC-40 was 1.68 (layered) and 1.91 mm (column).
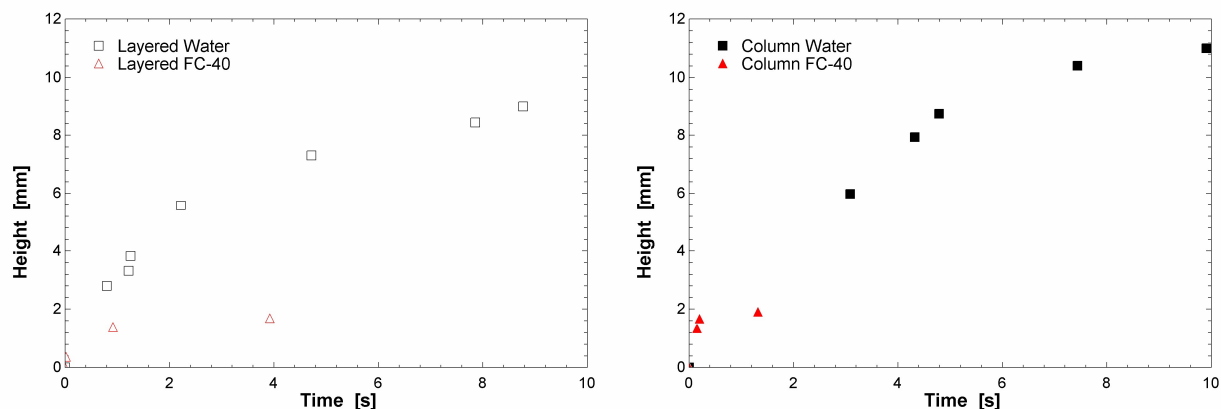
Figure 10: Height vs. time for the 1.0 mm column and layered wicks when using both water and FC-40

Figure 11 shows the rate at which the fluid rose in the 1.75 mm square layered wick with respect to time. The 1.75 mm square column wick was unable to pull either fluid vertically into the wick structure. The layered wick reached a max height when using water of 5.64 mm and a max height when using FC-40 of 1.07 mm. The smaller, tighter packed wick (i.e., 1.0 mm triangle) performed almost twice as well as the larger, looser packed wick (i.e., 1.75 mm square).
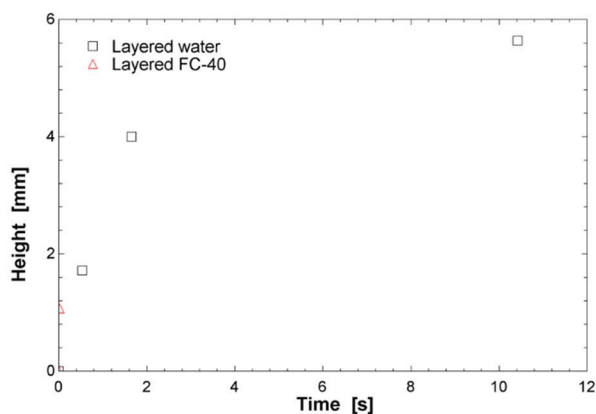
Figure 11: Height vs. time for the 1.75 mm square layered wicks using both water and FC-40

Once the data collected from the rate-of-rise test were analyzed with max height and time, the least square method described above was used to calculate the permeability and effective pore radius. The least square method was used on the water experiments because the larger height and time values give more confidence in the analysis. Table 2 presents the permeability and effective pore radius values in μm^2 and μm, respectively. Because the 1.75 mm square wick was unable to wick either fluid, calculating the values of permeability and effective pore radius were not possible.

Interior wick geometry impacted performance. The 1.0 mm triangle layered wick is tighter packed, yielding a smaller effective pore radius. This makes it easier to pull the fluid into the wick, while the larger permeability allows for the fluid to flow through the wick easier, allowing for higher heights, as shown by the performance of the 1.0 mm triangle column wick. The 1.75 mm square wicks show another interesting effect. The column wick was unable to wick any fluid into the wick, suggesting that the capillary force of the wick was unable to overcome the

gravitational and friction forces. Looking closer at the layered wick, shown in Figure 12, the open space of the structure is much smaller along the wall than it is in between layers of the wick. This suggests that the wick is able to pull the fluid into the wick along the wall where the capillary action is acting and then the fluid is moved and held in the larger spaces away from the wall. This is supported by the lack of performance by the column wick where the pores are too big to allow for capillary action to pull fluid into the wick.

Table 2: Permeability and effective pore radius of layered and column wicks

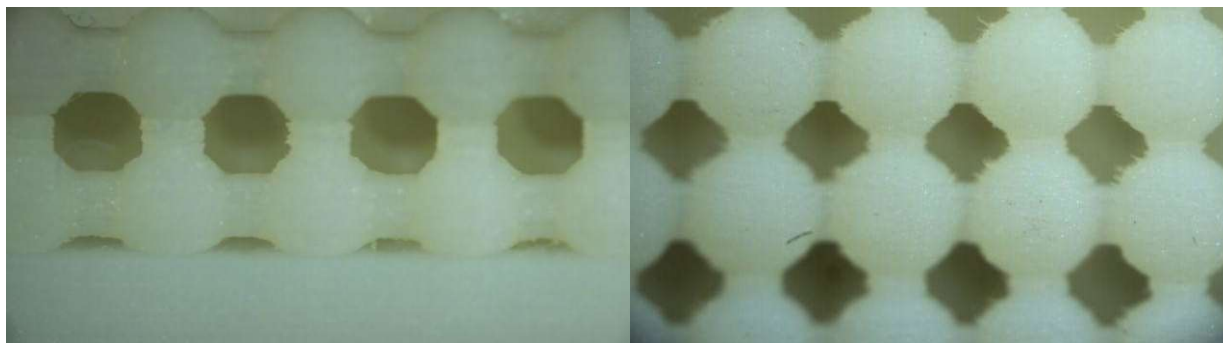| Wick type	Layered		Column	
	Permeability [µm²]	Effective Pore Radius [µm]	Permeability [µm²]	Effective Pore Radius [µm]
1.0 mm triangle	3.00	130.1	77.8	1099
1.75 mm square	0.95	221.1	N/A	N/A

Figure 12: Side by side comparison of pore size of the 1.75 mm layered (left) and column (right)

3.2 Additive manufacturing challenges
Figure 13 shows two examples of the challenged involved with additive manufacturing with polymers. The first example shows a structure that seems to be printable, but the small tight pores on the inside of the structure made it very difficult to clean out, as shown by the lighter colored particles. The lighter colored particles were support structures which are typically blown out after the structure is printed. The second example shows a structure that, as shown in the CAD file, should print with spaces between each column. However, the resolution of the printer was larger than the space between the columns that was trying to be printed. The desired spacing between the pillars was 0.06 mm, notably smaller than the resolution of the printer (i.e., 0.28 mm), resulting in overlap between each pillar. It is important to keep in mind during design of 3D printed structures, especially wicks where the pore size is important for performance.
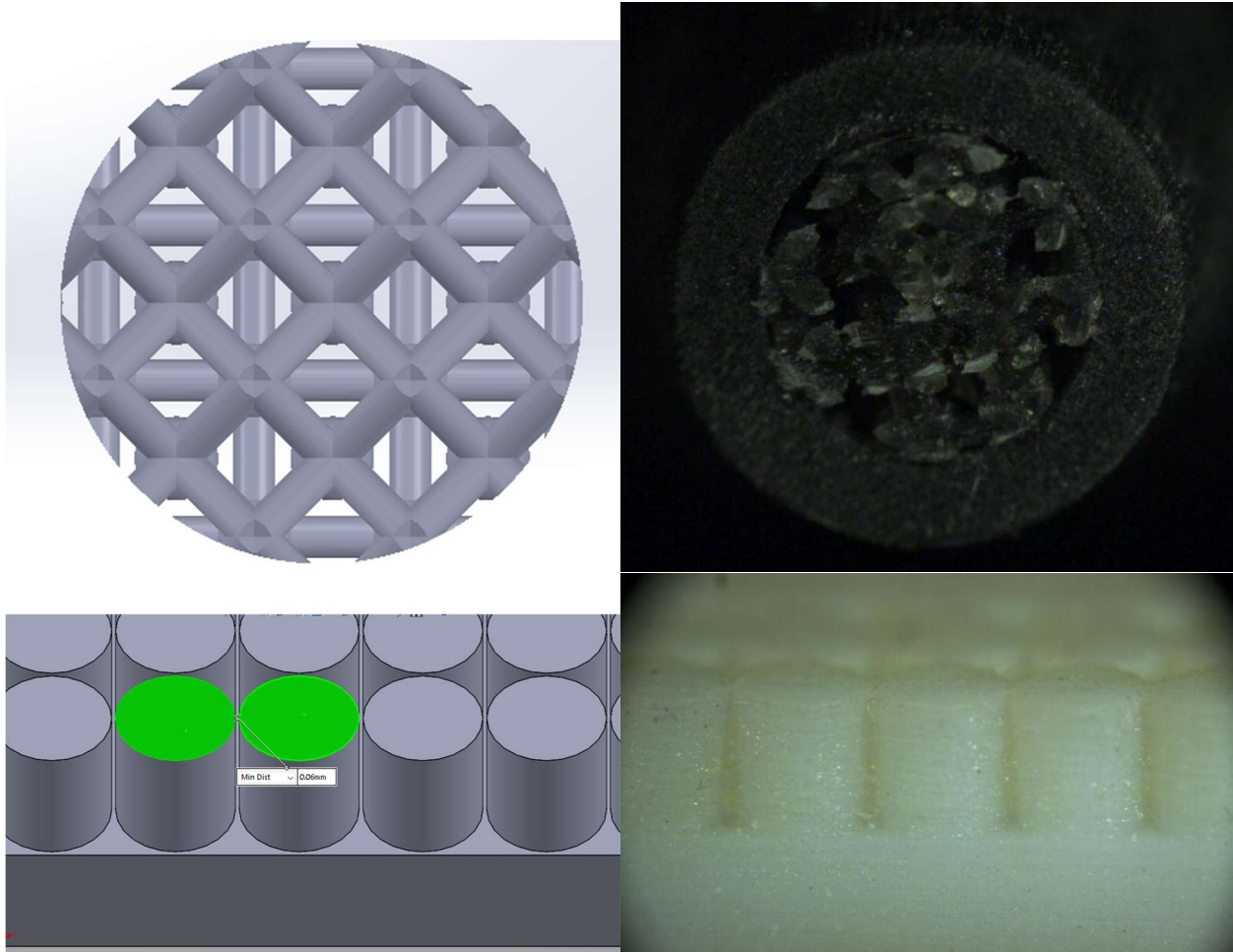
Figure 13: Examples of 3D printing errors

4. CONCLUSIONS

This research investigated two test structures (i.e., layered and column) and two wick structures (i.e., 1.0 mm triangle and 1.75 mm square). All four structures were tested with water and a low surface tension fluid FC-40. Rate-of-rise tests were conducted on all four wicks using both fluids. Both variants of the 1.0 mm wicks performed almost twice as well as the 1.75 mm wick structures. The 1.75 mm column wick was unable to wick either fluid because of its large pores, while the 1.75 mm layered wick was able to wick both fluids because the small pores created along the support wall of the wick were able to move the fluid using capillary action while the larger pores away from the wall held the wicked fluid. A brief discussion on the challenges of 3D printed was included. There are challenges involved with building structures that work effectively with passively moving liquid and are able to be constructed with the building resolution of the 3D printer. The other side of this is that while more complicated wicks can be more effective (e.g., the 1.0 mm wicks), they are harder to print and clean out (e.g., the first example from Figure 5). These tradeoffs must be considered as wicks structures are being designed to be used in heat pipes and other heat transfer applications.

NOMENCLATURE

g	gravity	(m/s^2)
K	permeability	(μm^2)
r_{eff}	effective pore radius	(μm)
t	time	(s)
V	volume	(m^3)
x	height	(m)

ΔP	change in pressure	(Pa)
ε	porosity	(-)
μ	liquid viscosity	(Pa s)
ρ	liquid density	(kg/m^3)
σ	surface tension	(N/m)

Subscript

cap	capillary pressure
hs	hydrostatic pressure
f	pressure loss due to friction
solid	solid material of wick
total	total volume encompassed by wick

REFERENCES

Adera, S., Antao, D., Raj, R., & Wang, E. N. (2016). Design of micropillar wicks for thin-film evaporation. *International Journal of Heat and Mass Transfer, 101*, 280-294.

Albu, N., Keese, J., & Hwang, G. (2019). *Bimodal, thin wick structures for high heat flux two-phase thermal control systems*.

Esarte, J., Blanco, J., Bernardini, A., & San-José, J. (2017). Optimizing the design of a two-phase cooling system loop heat pipe: Wick manufacturing with the 3D selective laser melting printing technique and prototype testing. *Applied Thermal Engineering, 111*, 407-419.

Hale, R., Ranjan, R., & Hidrovo, C. (2014). Capillary flow through rectangular micropillar arrays. *International Journal of Heat and Mass Transfer, 75*, 710-717.

Holley, B., & Faghri, A. (2006). Permeability and effective pore radius measurements for heat pipe and fuel cell applications. *Applied Thermal Engineering, 4*(26), 448-462.

Horner, D., Ravi, S., & Moghaddam, S. (2014). Monoporous micropillar wick structures, II-optimization & theoretical limits. *Applied Thermal Engineering, 73*(1), 1378-1386.

Huang, G., Yuan, W., Tang, Y., Zhang, B., Zhang, S., & Lu, L. (2017). Enhanced capillary performance in axially grooved aluminium wicks by alkaline corrosion treatment. *Experimental Thermal and Fluid Science, 82*, 212-221.

Jafari, D., Wits, W. W., & Geurts, B. J. (2017). *An investigation of porous structure characteristics of heat pipes made by additive manufacturing*. Paper presented at the 2017 23rd International Workshop on Thermal Investigations of ICs and Systems (THERMINIC).

Jafari, D., Wits, W. W., & Geurts, B. J. (2018). Metal 3D-printed wick structures for heat pipe application: Capillary performance analysis. *Applied Thermal Engineering, 143*, 403-414.

Li, C., & Peterson, G. (2006). Evaporation/boiling in thin capillary wicks (II)—effects of volumetric porosity and mesh size. *Journal of heat transfer, 128*(12), 1320-1328.

Li, C., Peterson, G., & Wang, Y. (2006). Evaporation/boiling in thin capillary wicks (l)—wick thickness effects. *Journal of heat transfer, 128*(12), 1312-1319.

Ravi, S., Horner, D., & Moghaddam, S. (2014). Monoporous micropillar wick structures, I-Mass transport characteristics. *Applied Thermal Engineering, 73*(1), 1371-1377.

Tang, Y., Deng, D., Lu, L., Pan, M., & Wang, Q. (2010). Experimental investigation on capillary force of composite wick structure by IR thermal imaging camera. *Experimental Thermal and Fluid Science, 34*(2), 190-196.

ACKNOWLEDGEMENTS